Journal of Advanced Biomedical Sciences

Journal of Advanced Biomedical Sciences
https://jabs.fums.ac.ir/
Online ISSN: 2783-1523

Fasa University of Medical Sciences

Ultra-sensitive Two-dimensional Photonic Crystal Biosensor for Oral Cancerous Cell Detection

Hossein Ghaforyan

Department of Physics, Payame Noor University (PNU), Tehran, Iran

Article Info

Article Type:
Research Article

Article history:
Received
23 Apr 2024
Received in revised form
01 May 2024
Accepted
05 May 2024
Published online
14 Jun 2024

Publisher
Fasa University of Medical Sciences

Abstract

Background & Objectives: Over the past two decades, biophotonic sensors based on two-dimensional (2D) photonic crystals (PhCs) have garnered significant attention in cancer diagnosis. This technology has become a crucial tool in early cancer detection and treatment response monitoring due to its ability to detect minute changes in biomarker concentrations and molecular interactions. The development of these sensors through advanced nano and microfabrication techniques has significantly improved diagnostic accuracy and speed, promising substantial enhancements in therapeutic outcomes for cancer patients.

Materials & Methods: A biosensor based on a 2D PhC was designed and simulated for the detection of oral cancer cells in a sample. The biosensor, structured with silicon rods in air using the Finite-Difference Time-Domain tool, utilizes five rods as an analyte for detecting normal and cancerous cells, thereby evaluating the sensor's performance.

Results: The variation in the transmission spectrum was studied to detect the presence of malignant cells in the test sample. The sensor's structural parameters were carefully adjusted to enhance its sensitivity, a crucial factor in the accurate detection of cancerous cells. Two critical parameters, Q-factor and sensitivity, were derived from the results. The sensor achieved a sensitivity of 1148 nm/RIU with a Q-factor of 193.

Conclusion: The designed biosensor demonstrates superior accuracy and sensitivity in identifying both malignant and normal cells in the test sample, making it suitable for real-time deployment in point-of-care applications.

Keywords: Photonic crystals, Cancers, Biosensors, Diagnosis

Cite this article: Ghaforyan H. Ultra-sensitive Two-dimensional Photonic Crystal Biosensor for Oral Cancerous Cells Detection. J Adv Biomed Sci. 2024; 14(3): 200-209.
DOI: 10.18502/jabs.v14i3.16357

Introduction

Cancer, responsible for more fatalities than all other major diseases combined, is projected to affect over 20 million patients by 2025, particularly in low-income countries (1). The detection and recognition of various cancerous cells during their early stages present significant challenges for pathologists and medical professionals. The efficacy of microscopic imaging techniques in identifying cancer cells varies among patients, contingent upon the level of experience, meticulous observation, and accurate predictions of the examining professional (2). Oral cancerous cells, originating from the tissues of the mouth or throat, are characterized by aberrant, uncontrolled cell proliferation, which can progress to malignancy. These cells may manifest in diverse regions of the oral cavity, including the lips, tongue, cheeks, and floor of the mouth. In their initial stages, oral

Corresponding Author: **Hossein Ghaforyan,** Department of Physics, Payame Noor University (PNU), P. O. Box 19395-4697, Tehran, Iran.
Email: hghaforyan@pnu.ac.ir

[Downloaded from jabs.fums.ac.ir on 2026-11-10]

[DOI: 10.18502/jabs.v14i3.16357]

cancer may present as persistent sores, lumps, or areas of discoloration. Risk factors for oral cancer encompass tobacco use, excessive alcohol consumption, human papillomavirus (HPV) infection, and prolonged sun exposure to the lips. Early detection and diagnosis are crucial for enhancing prognosis and survival rates, underscoring the importance of efficient and accurate detection methods.

A plethora of analytical and experimental techniques have been developed to detect cancerous cells in their nascent stages (3-7). Various approaches are available to identify and localize cells based on their biophysical characteristics (8-11). The optical properties of cells serve as one of the essential biological factors in distinguishing between healthy and cancerous cells. The refractive index (RI) method is a widely employed detection technique, providing valuable insights into cell abnormalities. Refractometry methods enable the measurement of RI values for individual live cells based on their optical characteristics (12-14). Photonic crystal (PhC) biosensors are devices that harness the properties of PhC to detect and analyze biological substances. PhCs are materials exhibiting periodic fluctuations in their RI, thereby creating a photonic bandgap that influences the transmission of electromagnetic waves, including light. These crystals can be engineered with specific characteristics suitable for biosensing applications. Analogous to the electronic bandgap in semiconductors, the periodic structure of PhCs generates a bandgap that prohibits the propagation of specific light wavelengths (15-19). The photonic bandgap undergoes alterations when the RI of the surrounding medium changes due to biomolecules binding to the PhCs surface. By monitoring these changes in the photonic bandgap, the biosensor can detect fluctuations in concentration or the presence of biomolecules. The introduction of a defect in this periodic structure, such as a missing or modified rod, engenders localized resonant modes within the bandgap. These resonant modes manifest as sharp peaks in the transmission spectrum of the PhCs. When the RI of the sample changes (e.g., due to cancerous cells binding to the biosensor's surface), it alters the local optical environment of the PhC. This change in the local RI affects the resonant conditions of the defect mode, resulting in a shift in the resonant peak wavelength. The magnitude of this shift is directly proportional to the extent of the RI change (20-22). The position of the resonant peak in the transmission spectrum can be precisely measured, and any shift in this peak can be correlated with the RI change in the sample, facilitating the quantification of the amount and type of biological material (e.g., cancerous cells) present. By optimizing the design parameters of the PhC, such as the lattice constant, rod radius, and defect size, the sensitivity to RI changes can be maximized. A high-quality factor (Q-factor) resonant cavity within the PhC ensures that even minute changes in the RI result in significant shifts in the resonant peak, enabling the detection of low concentrations of cancerous cells. Despite the inherent challenges, ongoing research aims to address the difficulties associated with PhC sensors. These biosensors hold considerable promise for a wide range of biosensing applications, particularly in differentiating between benign and malignant cells (23-25). Lee et al. have demonstrated that PhC biosensors can detect protein biomarkers at concentrations as low as femtomolar levels, highlighting their potential for early cancer detection and improved patient outcomes (26). Furthermore, Rakavandi et al. have illustrated the development of a 2D PhC biosensor capable of distinguishing between benign and malignant cells based on subtle differences in their optical properties (27).

The diminutive size and highly accurate sensing capabilities of PhC sensors have rendered them increasingly prevalent in biosensing

[Downloaded from jabs.fums.ac.ir on 2026-11-10]
[DOI: 10.18502/jabs.v14i3.16357]

applications. In recent years, a plethora of PhC biosensors have been developed and investigated for various sensing applications. Among the diverse types of PhC sensors, two-dimensional (2D) PhCs are preferred due to their practical design and feasible fabrication. With the aid of advanced VLSI and micromachining techniques, 2D PhC sensors can be fabricated in real-time.

The design and methodology for creating biosensors with PhCs that exhibit superior optical properties present significant challenges. Through judicious selection of materials for the sensor's construction, it is possible to precisely control the light's characteristics within the PhC (28). A distinctive attribute of PhCs is the photonic bandgap (PBG), which can inhibit light propagation for a specific frequency band (29). By introducing a structural flaw, the propagation of light through the PhC can be modulated. 2D PhCs are intricate arrangements of materials that exhibit a periodic pattern in two dimensions. Analogous to how semiconductors affect the flow of electrons, these structures are engineered to manipulate and regulate the propagation of light. The composition of a 2D PhC engenders a particular optical environment that gives rise to unique optical features. What distinguishes a 2D PhC is its periodicity—the recurring arrangement of components on a regular grid. This periodic structure results in the photonic bandgap, which is a range of wavelengths or frequencies of light that the PhC prohibits from propagating through it (30).

The bandgap in PhCs pertains to a spectrum of light wavelengths or frequencies that cannot traverse the crystal. Constructive interference occurs when the wavelength of the light coincides with the periodicity of the PhC structure. This results in enhanced interactions between the incident light and the crystal, causing that wavelength to be reflected or absorbed. Conversely, destructive interference occurs at wavelengths that do not match the periodicity, creating a gap in the permitted wavelength range known as a photonic bandgap. The effects of the photonic bandgap on the behavior of light in the crystal are profound. The bandgap is essential for applications such as lasers because it inhibits the propagation of certain wavelengths, which amplifies a particular wavelength that forms the foundation of laser operation. Wavelengths within the bandgap are effectively prohibited from propagating through the structure. However, wavelengths outside the bandgap are permitted to propagate rapidly. Consequently, crystal characteristics can be engineered by designers to modulate the behavior of light. The regulation of light propagation in 2D PhC has numerous practical applications. By adjusting the periodicity and arrangement of materials, designers can create optical filters, waveguides, and resonators.

Materials and Methods

The sensor described in this paper employs a 2D square grating lattice with a rods-in-air arrangement. The sensor incorporates a waveguide, which includes defects created by removing necessary rods. These regions facilitate the propagation of light. The normal and cancerous cells are immersed in the analyte (Figure 1). Light is sourced and detected from the ends of the PhC to detect the interaction of light with the test sample. The dielectric constant of the test sample, including normal and various cancerous cells, affects the propagation of light. This structure has been designed and optimized to achieve high sensitivity, enabling it to detect a variety of malignant cells in the sample under test. The sensitivity of the structure increases as the frequency of the propagated signal shifts farther away.

The designs of the proposed structures

The basic rods are arranged in a square lattice structure with an air configuration, as shown in Figure 1. These rods are strategically distributed both horizontally and vertically in the lattice region, with a lattice constant of 'a'.

[Downloaded from jabs.fums.ac.ir on 2026-11-10]
[DOI: 10.18502/jabs.v14i3.16357]

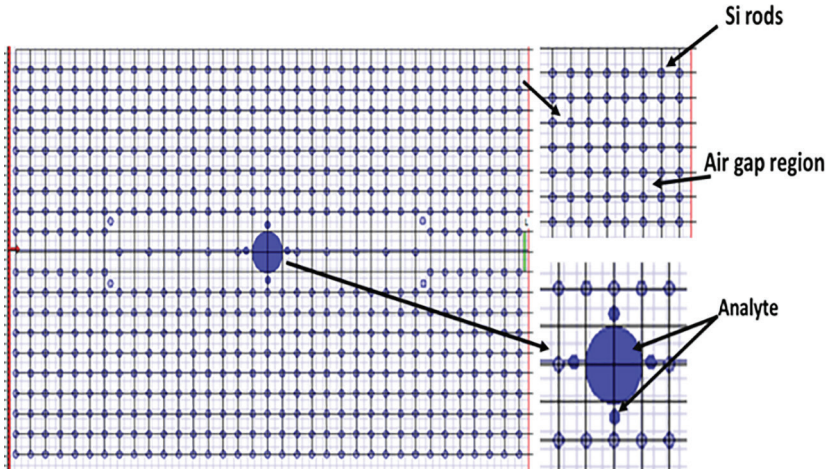


Figure 1. Designed biosensor based on the 2D PhC structure

What distinguishes this structure is the use of silicon material, with a dielectric constant of 3.45, as the rods in air structures. The radius of Si rods is 95 nm, and the area of the lattice structure is 228 μm^2. Additionally, the radius of the analyte rod is 550 nm. This unique design is the result of an optimization process that meticulously considers the rod radius and lattice, ensuring the structure's efficiency and effectiveness. The 2D PhC structure is created with precision using the Optiwave simulation tool. This tool is an essential and powerful component of our research (31). It employs the Finite-Difference Time-Domain (FDTD) method to solve the PhC structure. The tool is user-friendly, efficient, and effective in designing and simulating PhCs. It also enables us to analyze the behavior of photonic components and model polarization effects, scattering, diffraction, and light propagation. As a result, we gain a comprehensive understanding of nanoscale structures. The FDTD method, which forms the foundation of this tool, is based on Maxwell's time-varying curl equations along with their solutions. This method divides the spatial domain into a grid of cells, with electric and magnetic field components alternately placed in each cell. Consequently, the results of the FDTD method can be directly applied to the time evolution of electromagnetic fields. The models are matrix-free and can easily run in parallel on supercomputers. Additionally, the FDTD method naturally handles impulsive and nonlinear behaviors, although error sources are well-identified and can be constrained to certain levels (32). The adaptability of the FDTD method is a key feature, as it does not automatically require reformulation; instead, changes are typically made only to account for new and additional parameters if necessary, providing reassurance about its flexibility. The FDTD method simulates the time evolution of electric and magnetic fields across a spatial grid using Faraday's law and the Ampere-Maxwell law in time-domain form. Initially, the first two Maxwell's equations are obtained in a coupled and simultaneous manner and in parallel. The FDTD grid is usually generated in Cartesian coordinates with non-co-located and alternating electric and magnetic field components.

In this simulation, we used the transverse electric field mode (TE) where the electric field has only a z-component, E_z and the magnetic field have x and y components, H_x and H_y. Maxwell's curl equations in 2D for TE mode are:

$$\frac{\partial H_x}{\partial t} = -\frac{1}{\mu}\frac{\partial E_z}{\partial y} \quad (1)$$

$$\frac{\partial H_y}{\partial t} = \frac{1}{\mu}\frac{\partial E_z}{\partial x} \quad (2)$$

[Downloaded from jabs.fums.ac.ir on 2026-11-10]
[DOI: 10.18502/jabs.v14i3.16357]

$$\frac{\partial E_z}{\partial t} = \frac{1}{\varepsilon}\left(\frac{\partial H_y}{\partial x} - \frac{\partial H_x}{\partial y}\right) \quad (3)$$

Were the electric field has only a z-component, E_z and and the magnetic field has x and y components H_x and H_y. The FDTD method discretizes both time and space. We define a grid with spatial steps Δx and Δy, and a temporal step Δt. The fields are sampled at discrete points in space and time: $E_z(i, j, n)$, $H_x(i, j, n)$ and $H_y(i, j, n)$, where i and j are spatial indices, and n is the time index. The FDTD update equations are derived by approximating the spatial and temporal derivatives using finite differences (32) (Ref 33????).

$$H_x^{n+\frac{1}{2}}(i, j+\frac{1}{2}) = H_x^{n-\frac{1}{2}}(i, j+\frac{1}{2}) - \frac{\Delta t}{\mu \Delta y}[E_z^n(i, j+1) - E_z^n(i, j)] \quad (4)$$

$$H_y^{n+\frac{1}{2}}(i+\frac{1}{2}, j) = H_y^{n-\frac{1}{2}}(i+\frac{1}{2}, j) + \frac{\Delta t}{\mu \Delta x}[E_z^n(i+1, j) - E_z^n(i, j)] \quad (5)$$

$$E_z^{n+\frac{1}{2}}(i, j) = E_z^n(i, j) + \frac{\Delta t}{\varepsilon}\left[\frac{H_y^{n+\frac{1}{2}}\left(i+\frac{1}{2}, j\right) - H_y^{n+\frac{1}{2}}\left(i-\frac{1}{2}, j\right)}{\Delta x} - \frac{H_x^{n+\frac{1}{2}}\left(i, j+\frac{1}{2}\right) - H_x^{n+\frac{1}{2}}\left(i, j-\frac{1}{2}\right)}{\Delta y}\right] \quad (6)$$

Results

In this experiment, the five rods in the central region are filled with the sample under test. As light interacts with the sample throughout the structure, its propagation is facilitated through the waveguide. The RI of the sample varies with the presence of different cell types, and the light exhibits a resonant peak based on this RI. As the RI of the sample changes, the resonant peak of the transmission spectrum also shifts, reflecting the presence of different cell types. The experiment demonstrates that malignant cells typically possess a higher RI than normal cells, which enhances their detectability. The proposed work utilized five types of normal and cancerous cells, with their respective RIs tabulated in Table 1. A shift in the resonant peak towards higher wavelengths can be observed with increasing sample RI. It is evident from the experiment that the most prevalent method for identifying cancerous cells is based on varying RI values. The literature suggests that most cancer cells exhibit higher RI than normal cells. Crucially, the experiment underscores that early detection of these cancer cells can be life-saving.

The cavity is filled with the sample under test, and light is directed onto it. A Gaussian pulse laser, operating in the range of 1300 to 1400nm, is positioned at the left side of the bus waveguide, with light passing through the structure precisely at the resonance peak. Figure 2 illustrates the propagation and confinement of light through the structure, depicting light propagating and being confined through the bus waveguide and analyte regions. After traversing the structure, the light reaches the detector.

The RI of the sample varies depending on the presence of different cell types - normal and cancerous. When light interacts with the

Table 1. Refractive index of various Oral cell types

Oral Cell Types	Refractive Index		$\Delta N = n_{Cancer} - n_{Normal}$
	n_{Normal}	n_{Cancer}	
Type A	1.343	1.369	0.026ΔΔ
Type B	1.344	1.371	0.027
Type C	1.345	1.372	0.027
Type D	1.348	1.377	0.029
Type E	1.351	1.378	0.027

[Downloaded from jabs.fums.ac.ir on 2026-11-10]
[DOI: 10.18502/jabs.v14i3.16357]

test sample, it produces a resonant peak based on the sample's RI. As the RI of the sample fluctuates, the resonant peak of the transmission spectrum also shifts, indicating the presence of different cell types. This phenomenon is clearly demonstrated in the transmission plot in Chart 1, which represents various samples under examination. The RI of type A cells is minimal and increases progressively with type B, type C, and so on. As the sample's RI increases, the resonant peak shifts to higher wavelengths.

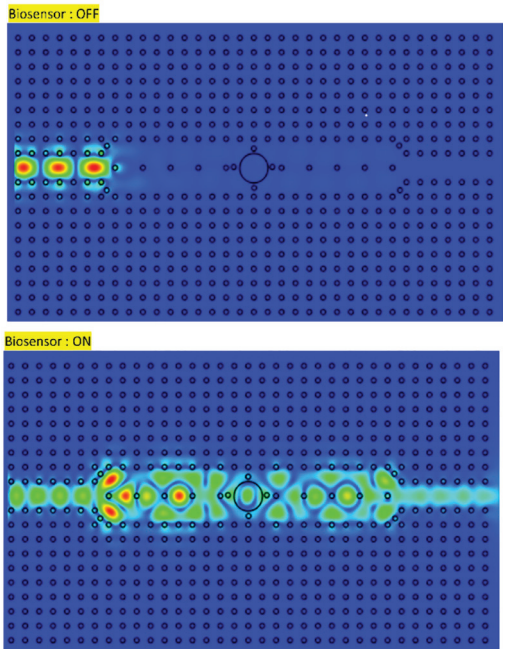


Figure 2. Light propagation and confinement through the waveguide

The following information can be utilized to identify the presence of cancerous cells in samples. Chart 2 indicates that the presence of various normal and cancerous oral cells with different RI values causes the resonance peak wavelength to shift to higher wavelengths. For type A cells, if normal, the resonance peak occurs at 1312 nm; however, if cancerous, the resonance peak shifts by 27 nm to 1339 nm. Similarly, for type B cells, the resonance wavelength peak for normal cells occurs at 1313 nm, while for the cancerous sample of the same cell type, it occurs at 1341 nm, indicating a displacement of 28 nm. In the case of type C cells, the resonance

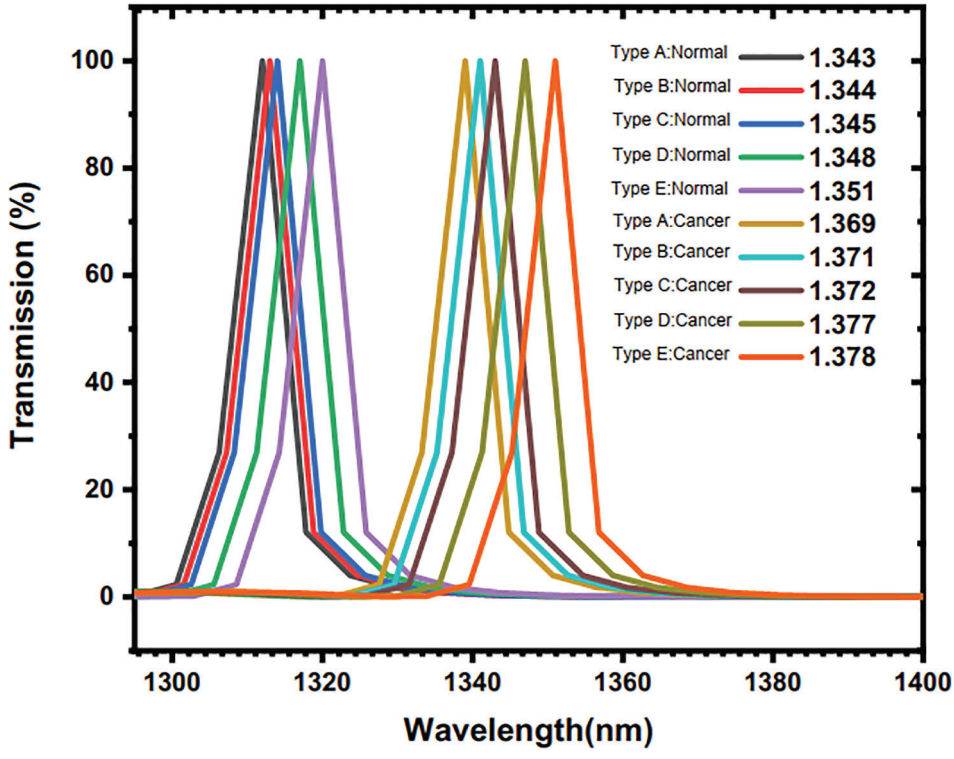


Chart 1. Transmission Curve of the light passing through the proposed structure with various types of cells under test

[Downloaded from jabs.fums.ac.ir on 2026-11-10]
[DOI: 10.18502/jabs.v14i3.16357]

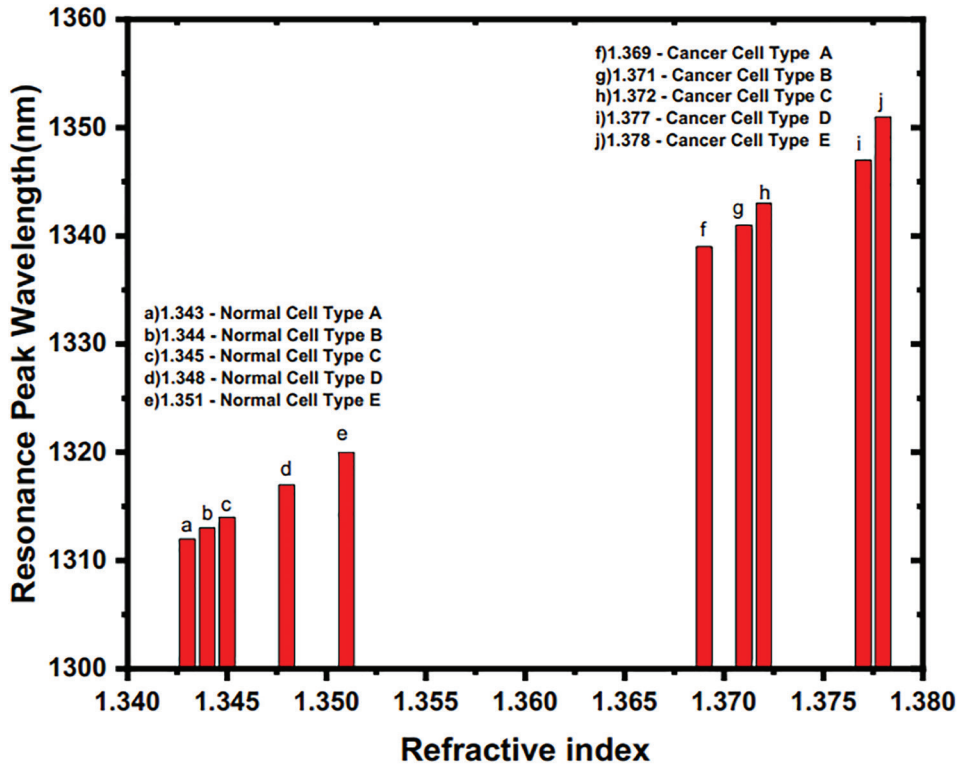


Chart 2. Resonant wavelength peak variation with the different refractive index of Oral normal and cancerous cells

wavelength peak occurs at 1314 nm for normal cells and, after a shift of 29 nm, at 1343 nm for its cancerous counterpart. When the test sample consists of type D cells, the resonance wavelength peak for normal cells occurs at 1317 nm, but for the cancerous type, it shifts to 1347 nm. Finally, for type E cells, resonance occurs at 1320 nm for normal cells, while for the cancerous sample, the resonance wavelength shifts to 1351 nm.

The sensitivity and Q-factor are the two most significant parameters that determine the sensor's performance and accuracy. Sensitivity refers to how responsive the proposed sensor is to the presence of malignant cells in the sample, while the Q-factor measures how accurately the sensor detects minute changes in the sample's RI. These two vital factors represent the performance of the proposed design. The sensitivity and Q-factor values can be calculated from the obtained results using the following formulae and plotted, as shown in Chart 3 and 4. The change in peak resonant wavelength due to a change in RI (ΔRI) is described by the following equations:

$$S = \frac{\Delta\lambda_{RW}}{\Delta RI} \quad (7)$$

$$Q = \frac{\lambda_{RW}}{\lambda_{FH}} \quad (8)$$

where $\Delta\lambda_{RW}$ is the change in peak resonant wavelength, ΔRI is the change in RI, λ_{RW} is the resonance wavelength, and λ_{FH} is the range of wavelengths where the filter transmits at least 50% of light at the center wavelength. Chart 3 illustrates the sensitivity for each biosensor for the detection of oral normal and cancerous cells. The sensitivity of the type A biosensor is 962, and with the increase in RI in cell types from B to E, the sensitivity increases, reaching a value of 1148.

[Downloaded from jabs.fums.ac.ir on 2026-11-10]
[DOI: 10.18502/jabs.v14i3.16357]

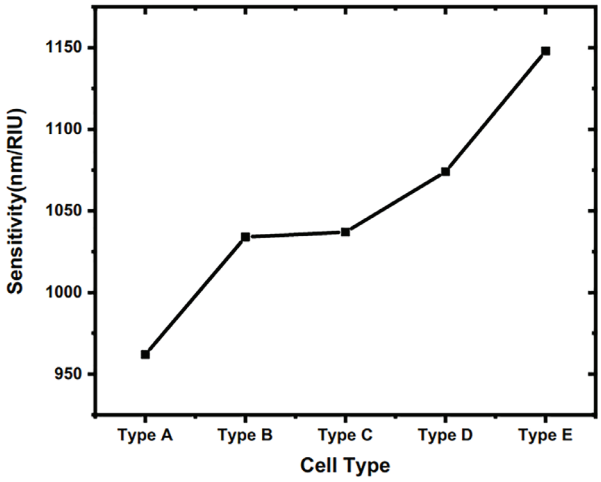


Chart 3. Proposed sensor sensitivity for the different biosensor types

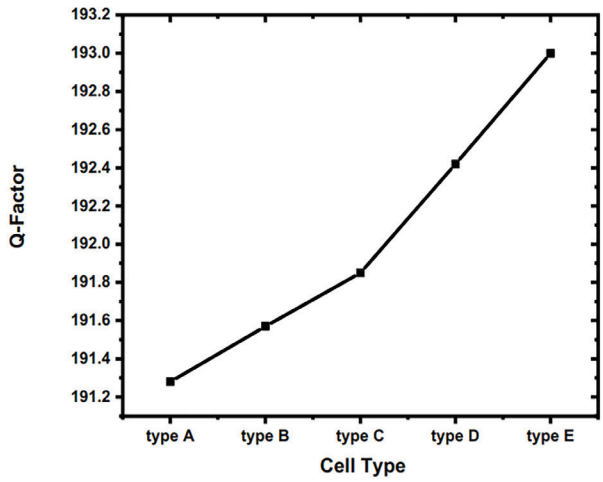


Chart 4. Proposed sensor Q-Factor for the different biosensor types

The proposed device is designed to enhance sensitivity rather than the Q-factor. Chart 4 displays the quality factor for each type of biosensor. The type A biosensor has a Qfactor of 191.28, which is comparable to 191.57, 191.85, 192.42, and 193 for other samples from B to E, respectively. These results demonstrate that the proposed structure is highly responsive to changes in RI and possesses a reasonable Q-factor.

Discussion and Conclusion

The proposed 2D PhC biosensor offers several advantages over existing cancer detection techniques, particularly in terms of sensitivity and practicality. We evaluated the sensor's effectiveness by measuring the transmission spectrum shift for a range of RI values. The shift in the wavelength of the transmission spectrum for the corresponding variation in the RI value of the analyte enables the sensing and detection of cancerous cells in the sample. By directly examining the transmission spectrum region, it is straightforward to identify the presence of cancerous cells in the sample. The suggested structure can be used in biochips for medical applications. It is straightforward to infer that by directly examining the transmission spectrum region, it is simple to identify the existence of oral cancer malignant cells in the sample. The proposed design achieved a sensitivity of 1148 nm/RIU and a Q-factor of 193. Furthermore, the proposed sensor design is compared with recently reported work, as tabulated in Table 2. Two important performance parameters of the biosensor, sensitivity and Q-factor, are compared. The comparison table demonstrates that the proposed sensor's accuracy and capability surpass those of existing sensors under similar circumstances. The designed

Table 2. Proposed sensor design compared with related work with the same refractive index of various types of normal and cancerous cells

Refractive index		Table 2 in Reference (34)		Present Work	
n_{Normal}	n_{Cancer}	Sensitivity	Q-Factor	Sensitivity	Q-Factor
1.343	1.369	2.308	141.31	962	191.28
1.344	1.371	2.370	141.32	1034	191.57
1.345	1.372	2.370	141.36	1037	191.85
1.348	1.377	2.345	141.45	1072	192.42
1.351	1.378	2.481	141.50	1148	193

[Downloaded from jabs.fums.ac.ir on 2026-11-10]
[DOI: 10.18502/jabs.v14i3.16357]

biosensor leverages the high RI contrast and precise structural control of PhCs to achieve high sensitivity. The sharp resonant peaks in the transmission spectrum are highly sensitive to minute changes in the RI, allowing for the detection of small quantities of cancerous cells. This can be especially beneficial for early-stage cancer detection where cell populations may be low. The sensor structure is simple and can be produced from a basic line defect and resonator, making it suitable for integration into biochips for medical applications. In conclusion, the proposed 2D PhC biosensor offers superior sensitivity and practicality compared to existing cancer detection techniques. Its ability to accurately identify both malignant and normal cells in test samples makes it appropriate for real-time deployment in point-of-care applications, potentially revolutionizing early cancer detection and diagnosis.

Acknowledgement

We extend our gratitude to Payam Noor University for providing the research funding for this project.

Funding

We would like to emphasize that this article was produced with financial support from Payame Noor University.

Ethical Considerations

In conducting simulations and research using FDTD tools, it is evident that the work primarily involves computational modeling rather than direct interaction with human subjects.

Code of Ethics

Research Project Number: 11749

References

1 Dillekås H, Rogers MS, Straume O. Are 90% of deaths from cancer caused by metastases? Cancer Med. 2019 ;8(12):5574-6.
2 Kaniyala Melanthota S, Kistenev YV, Borisova E, Ivanov D, Zakharova O, Boyko A, et al. Types of spectroscopy and microscopy techniques for cancer diagnosis: a review. Lasers Med Sci. 2022;37(8):3067-84.
3 Chakraborty S, Sharma G, Karmakar S, Banerjee S. Multi-OMICS approaches in cancer biology: New era in cancer therapy. Biochimica et Biophysica Acta Biochim Biophys Acta (BBA)-Molecular Basis of Disease. 2024;1870(5):167120.
4 Chung DC, Gray DM, Singh H, Issaka RB, Raymond VM, Eagle C, et al. A cell-free DNA blood-based test for colorectal cancer screening. New Engl J Med. 2024; 390(11):973-83.
5 Mahmoud A, El-Sharkawy YH. Multi-wavelength interference phase imaging for automatic breast cancer detection and delineation using diffuse reflection imaging. Sci Rep. 2024;14(1):415.
6 Karan S, Cho JH, Tran CT, Cho MY, Lee H, Naskar R, Hwang I, et al. Activatable near-infrared fluorescence and chemical exchange saturation transfer MRI multimodal imaging probe for tumor detection in vitro and in vivo. Sensand Actuators B: Chem. 2024 Aug 15;413:135839.
7 Keshavarz Motamed P, Abouali H, Poudineh M, Maftoon N. Experimental measurement and numerical modeling of deformation behavior of breast cancer cells passing through constricted microfluidic channels. Microsyst. Nanoeng. 2024;10(1):7.
8 Abderrahmane A, Senouci K, Hachemi B, Ko PJ. 2D gallium sulfide-based 1D photonic crystal biosensor for glucose concentration detection. Materials.2023;16(13):4621.
9 Ahn JC, Teng PC, Chen PJ, Posadas E, Tseng HR, Lu SC, et al. Detection of circulating tumor cells and their implications as a biomarker for diagnosis, prognostication, and therapeutic monitoring in hepatocellular carcinoma. J Hepatol. 2021 ;73(1):422-36.
10 Lu N, Tay HM, Petchakup C, He L, Gong L, Maw KK, et al. Label-free microfluidic cell sorting and detection for rapid blood analysis. Lab on a Chip. 2023;23(5):1226-57.
11 Raga S, Gowre SK, Miyan H, Sharan P. Two-dimensional photonic crystal biosensor based on gallium arsenide composite semi-conductive material for diabetes detection. Plasmonics. 2023; 18(4):1429-40.
12 Fathollahi-Khalkhali T, Shiri R. An ultra-sensitive refractive index-based photonic crystal biosensor with the coupled cavity-waveguide structure. Ind J Phys. 2023; 97(14):4427-37.
13 Sajan SC, Singh A, Sharma PK, Kumar S. Silicon photonics biosensors for cancer cells detection: A Review. IEEE Sensors J. 2023; 13;23(4):3366-77.

[Downloaded from jabs.fums.ac.ir on 2026-11-10]
[DOI: 10.18502/jabs.v14i3.16357]

14 Malek C, Al-Dossari M, Awasthi SK, Ismail MA, El-Gawaad NA, Sabra W, et al. High performance biosensor composed of 1D defective photonic crystal for sensing and detection of distinguished blood components. Opt. Quantum Electron. 2023; 55(3):196.
15 Rafiee E. Photonic crystal based biosensor for diagnosis of kidney failure and diabetes. Plasmonics. 2024; 19(1):439-45.
16 Zagaglia L, Zanotti S, Minkov M, Liscidini M, Gerace D, Andreani LC. Polarization states and far-field optical properties in dielectric photonic crystal slabs Opt Lett. 2023; 48(19):5017-20.
17 Ebrahimzadeh M, Ghaffari M, Ghaffari L. The Effect of External Magnetic Field on the Creation of Energy Levels Degeneracy in a Quantum Anti-Dot. Quarter J Optoelectronic. 2021; 3(1):81-8.
18 Moradi Dangi M, Mohammadzadeh Aghdam A, Karimzadeh R. Tunable optical filter with high performance based on 2D photonic crystal. J Comput Electron. 2023; 22(3):849-55.
19 Yang X, Hou S, Xie C, Wu G, Yan Z. High-performance photonic crystal fiber biosensor based on surface plasmon resonance for early cancer detection. Plasmonics. 2024; 19(2):675-85.
20 Ebrahimzadeh M, Salaki M. Investigation of Optical Properties of Ellipsoidal Metal Nanoparticles at Different Scales and Dielectric Environments. Quarter J Optoelectronic. 2021; 3(2):51-62.
21 De Almeida LC, de Sousa FB, Junior WG, Costa MB. 2D-FDTD Electromagnetic Simulation of an Ultracompact All-Optical Logic Gate Based on 2D Photonic Crystal for Ultrafast Applications. J Comm Inf Syst. 2024; 39(1):35-45.
22 Yashaswini PR, Gayathri HN, Srikanth PC. Performance analysis of photonic crystal based biosensor for the detection of bio-molecules in urine and blood. Mater. Today: Proceedings. 2023;80:2247-54.
23 Talebzadeh R, Beiranvand R, Moayed SH. Design and simulation of an all-optical Fredkin gate based on silicon slab-waveguide in a 2-D photonic crystal. Opt Quantum Electron. 2023;55(3):241.
24 Gowdhami D, Balaji VR. Analysis and design of photonic crystal malaria biosensor with double nanohole cavity resonator with ultra-high-quality factor. Opt. Quantum Electron. 2024;56(4):593.
25 Zhu J, Li T. Photonic crystal and Ti nanoparticles enhanced high-absorption GaAs thin-film solar cell. MatSci in Semicon Proc. 2024;176:108322.
26 Lee M, Fauchet PM. Two-dimensional silicon photonic crystal based biosensing platform for protein detection. Opt Express. 2007;15(8):4530-5.
27 Rakavandi P, Ehyaee A, Olyaee S. Design and analysis of a two-dimensional photonic crystal plus-shaped resonator for the detection of different cancerous cells and urine glucose. Mod Phys Lett B. 2023;37(33):2350158.
28 Liu Y, Hou X, Song Y, Li M. Bioinspired reflective display based on photonic crystals. Interd Mater 2024;3(1):54-73.
29 Butt MA, Khonina SN. Recent Advances in Photonic Crystal and Optical Devices. Crystals. 2024;14(6):543.
30 Khairulazdan NB, Menon PS, Zain AR, Berhanuddin DD. Optimization of photonic crystal structure by FDTD method to improve the light extraction efficiency in silicon. Chalcogenide Letters. 2022;19(7) 493-501.
31 Abdulwahhab AA, Mansour TS. Design and Analysis of BIMD Double Clad MMF-MZI Using Optiwave Simulation. Ir J Laser. 2021 Aug 20;20(1):1-5.
32 Zhang Z, Zhang W, Zeng L. Analyzing photonic space-time crystal with FDTD. Mod Phys Lett B. 2020;34(06):2050082.
33 Lavrinenko A, Borel PI, Frandsen LH, Thorhauge M, Harpoth A, Kristensen M, et al. Comprehensive FDTD modelling of photonic crystal waveguide components. Opt Express. 2004;12(2):234-48.
34 Gowda RB, Saara K, Sharan P. Detection of oral cancerous cells using highly sensitive one-dimensional distributed Bragg's Reflector Fabry Perot Microcavity. Optik. 2021; 244:167599.

[Downloaded from jabs.fums.ac.ir on 2026-11-10]
[DOI: 10.18502/jabs.v14i3.16357]